2

Conf-911132--6

38th Annual AVS Symposium & Topical Conference
Seattle, Washington
Nov. 11-15, 1991

SAND--91-1109C

DE92 003624

ION BEAM ANALYSIS FOR DEPTH PROFILING

J. A. Knapp, J. C. Barbour, and B. L. Doyle
Sandia National Laboratories
Albuquerque, New Mexico

Abstract

New techniques in the application of ion beam analysis to depth profiling in solids are briefly surveyed. These include: (1) non-Rutherford backscattering analysis using high energy beams, (2) Resonant Nuclear Reaction Analysis, (3) Time-of-Flight Elastic Recoil Detection Spectrometry, and (4) Heavy Ion Backscattering Spectrometry. The last can be used for very precise depth profiling in one configuration, or as a very sensitive trace contaminant analysis in another configuration.

DISCLAIMER

Introduction

Ion beam analysis has a long history as a powerful, non-destructive tool for profiling the composition of the near surface of solids. The most commonly available technique, Rutherford Backscattering Spectrometry (RBS), uses analysis beams of 1-2 MeV ^{4}He to give a depth resolution of ~ 15 nm and a sensitivity of $\sim 10^{13}$ atoms/cm^2, but is most useful for elements heavier than the substrate. In recent years, a variety of other analysis techniques have been developed to take advantage of the wider variety of ion beams that are available with modern accelerators, allowing profiling of light elements, better resolution, and better sensitivity. These include Elastic Recoil Detection (ERD) and Resonant Nuclear Reaction Analysis (RNRA). More recently, Time-of-Flight ERD (TOF-ERD) has been developed at several laboratories, which gives a depth resolution of 2 nm for light elements such as B and C. Furthermore, by detecting both recoiled ion energy and flight time, the depth profiles of light elements with only slightly different masses can be easily separated (including different isotopes of a single element). High Energy non-Rutherford Backscattering Spectrometry (HE-BS) is another technique which can be used to profile light elements under specific circumstances. Finally, Heavy Ion Backscattering Spectrometry (HIBS), can be used for highly accurate depth profiling in one configuration; or, in another configuration, provide extremely high sensitivity to heavy impurities on or near the surface of a light substrate such as Si.

Ion beam analysis (IBA) has both advantages and disadvantages when used for composition depth profiling in materials research. It is relatively non-destructive and repeatable, and allows tracking of composition changes as an experiment progresses. It is fast and quantitative, and with proper choice of ion beam and energy, useful for a broad range of elements. The main disadvantage of IBA has been its dependence on large, expensive ion accelerators for the beam source, but for the simpler techniques this has been largely overcome with the availability of small accelerators. At the same time, new generations of large accelerators have enabled the development of new modes of IBA, such as Time-of-Flight ERD, which would not otherwise be possible.

A complete review of IBA is well beyond the scope of this paper, and in any case many excellent reviews of the field are available.[1-5] Here we will briefly examine recent extensions to the techniques of IBA, and provide examples of their application to problems of interest in material analysis, particularly for depth profiling. Three of these, HE-BS, RNRA, and TOF-ERD, are techniques using high energy beams for depth profiling, while another, HIBS, is a low energy, heavy ion beam technique which can be used for either depth profiling or as an extremely sensitive trace element detector, depending on the configuration.

Principles of Ion Beam Analysis

The key features of ion beam analysis are illustrated in Fig. 1, which is a schematic of a basic RBS arrangement. An ion beam of energy E_0 is incident on the sample at angle θ_1. As the beam traverses the sample, it loses energy through interactions with the substrate. If an ion passes close enough to a target atom it will undergo a large-angle scattering event, with an energy loss determined by simple kinetics. The energy after scattering is:

$$E_1 = K_M E_0 \qquad \text{(eq. 1)}$$

where K_M is the backscattering kinematic factor:

$$K_M = \left\{ \frac{M_1 \cos\theta + \sqrt{M_2^2 - M_1^2 \sin^2\theta}}{M_1 + M_2} \right\}^2 \qquad \text{(eq. 2).}$$

Here M_1 is the mass of the incident particle, M_2 the mass of the target atom, and θ the backscattering angle. The dependence of the recoiling particle energy on the mass of the target atom gives RBS mass selectivity. The number of particles scattered in the direction of the detector determines the yield of counts from that particular target mass, and for the proper energy range is given by Rutherford's formula[6], as transformed from center-of-mass to a laboratory frame of reference differential scattering cross-section by Darwin[7]:

$$\frac{d\sigma}{d\Omega} = \left(\frac{Z_1 Z_2 e^2}{2E \sin^2\theta} \right)^2 \frac{\left\{ \cos\theta + \left[1 - \left(\frac{M_1}{M_2} \sin\theta \right)^2 \right]^{1/2} \right\}^2}{\left[1 - \left(\frac{M_1}{M_2} \sin\theta \right)^2 \right]^{1/2}} \qquad \text{(eq. 3)}$$

where Z_1 and Z_2 are the atomic numbers of the projectile and target atom, e is electron charge, and E is the energy of the particle immediately before scattering. The average scattering cross section, σ, is defined as

$$\sigma = \frac{1}{\Omega} \int \frac{d\sigma}{d\Omega} d\Omega \qquad \text{(eq. 4)}$$

where the integration is over Ω, the finite solid angle spanned by the detector.

After scattering, the backscattered particle continues to lose energy through substrate interactions, until it exits the sample. The final energy at the detector is determined both by the mass of the target atom and the energy loss incurred by the incident particle penetrating and exiting the sample. The depth, x, of the target atom can be deduced, using the known rates of energy loss (dE/dx), by calculating the total energy loss (ΔE) along the inward and outward paths. An approximate formula, using the average energy losses for the inward path and the outward path is:

$$\Delta E = K_M E_0 - E_1 = \left[\frac{K}{\cos\theta_1} \left.\frac{dE}{dx}\right|_{in} + \frac{1}{\cos\theta_2} \left.\frac{dE}{dx}\right|_{out} \right] x \qquad \text{(eq. 5).}$$

The rates of energy loss are experimentally determined; algorithms to produce smooth functions of particle energy and the necessary calculations to determine a depth scale have been incorporated into analysis programs such as RUMP[8] and SCATT.[9] The term in brackets in eq. 5 is often called the stopping power.

Although these equations are specific to RBS, the same principles apply to all ion beam analyses. In general, obtaining information about depth profiles requires measurement of the energy loss of a particle traversing the material, and then performing computations using measured or calculated stopping powers. In backscattering experiments, energy loss for the beam particle, both before and after scattering, is measured. In nuclear reaction analyses, energy loss is measured for the incident beam, or in some cases a reaction product ion. For elastic recoil detection, energy loss for a scattered target atom is measured. In all cases, the extracted depth scale is an areal density in units of atoms/cm^2, since the analyses are insensitive to density. Note that the areal density is just the volume density times the depth.

Non-Rutherford Backscattering Spectrometry

Table 1 summarizes the various IBA techniques useful for depth profiling. By far the best known IBA technique is RBS, and modern accelerator technology has allowed the construction of stand-alone RBS units which fit conveniently into a reasonable-size laboratory, making the technique more generally available. The ultimate sensitivity of RBS is limited to $\sim 10^{13}$ atoms/cm^2, primarily due to detector signal pileup and system noise. RBS is most useful for elements which are heavier than the substrate, since the yield from lighter elements is not only smaller (from the Z dependence in the scattering cross section, eq. 3), but also overlaps yield from the substrate. Thus an As implant profile in Si is easily extracted, but a C profile is difficult.

The limitation to detecting and quantifying the presence of elements heavier than the substrate is a serious difficulty for many experiments. An extension to RBS which can alleviate this problem for specific cases is HE-BS, which uses higher energy ion beams, chosen such that the scattering cross-section for the light element of interest is substantially higher than Rutherford. At higher energies, the scattering cross-sections for the heavier elements decrease as $1/E^2$ according to eq. 3, but σ for the light elements is generally non-Rutherford. These cross-sections often become larger than Rutherford, can be highly structured, and are different for each beam-particle/target-atom pair. Figure 2 shows the energy dependence of the scattering cross-section for ^4He incident on ^{16}O;[10] there are many sharp resonances evident as well as a number of broader regions where the cross-section is substantially above that given by the Rutherford formula (i.e., above $\sim$2.2 MeV the cross-section deviates from Rutherford). Since the energy at which the scattering becomes non-Rutherford increases with the Z of the target atom, it is often possible to choose an analysis energy for which the scattering (hence, the yield) from the light element of interest is greatly enhanced relative to the scattering from a heavier substrate, greatly improving signal to background for the analysis of the light element. It is also desirable to choose a region where the energy dependence is flat so that the yield/atom will be constant over a useful depth.

A good choice of energy for using ^4He to measure ^{16}O is 8.7 MeV, as illustrated by Fig. 3, where the backscattered α-particle energy (K_ME) is given along the top axis. In this example, a layer of Eu-Ba-Cu-O high temperature superconductor has been deposited on $SrTiO_3$.[11] At normal RBS energies of 1-2 MeV He, the O signal is too small to obtain an accurate quantification of the O content. Near 8.7 Mev, on the other hand, the scattering yield from O is 22 times Rutherford and flat for a useful width of $\sim$600 keV, which corresponds to an analysis range of $\sim 2\ \mu m$ for these materials. The oscillations in O yield at lower channels in Fig. 3 are due to the variations in the O cross-section at lower energies (i.e. deeper in the substrate). However, for a typical analysis of thin-film superconductors HE-BS at this energy allows the determination of an oxygen profile throughout the film with a depth resolution of $\sim 0.05\ \mu m$.

Another example of HE-BS is given in Fig. 4, where an Fe sample has been implanted with $2x10^{17}$ atoms/cm^2 of both Ti and C.[12] Again, at low energies the C profile would be difficult to measure accurately, but at 6 MeV the yield is 50 times Rutherford and reasonably flat, allowing more accurate profiling for C than for the Ti, whose cross-section is still Rutherford.

Other beam-target combinations which have proven useful for HE-BS are: 3.5 MeV ^4He analysis of N, with a cross-section which is twice Rutherford, and 3.7 MeV ^4He analysis of B, with a cross-section which is 3.3 times Rutherford. These have been successfully used for

determining elemental compositions in silicon nitride and boron nitride thin films. Many more examples could be given[13], but the technique is similar for all: a beam species and energy is chosen which enhances the yield from the light element of interest. Ideally, an energy should be chosen for which the cross-section is relatively flat over a range of energies. References 1,4 and 13 can be used as a starting place for finding an appropriate beam-target combination. In practice, some experimentation with energy is required, since the cross-section curves are published for only limited sets of conditions. For the same reason, yield calibrations should be performed with known standards once a configuration is decided upon.

Heavy Ion Backscattering Spectrometry

For many new problems in materials research, particularly for contamination control in microelectronics, the sensitivity of RBS is not nearly good enough to be useful. New generations of VLSI will require that levels of impurities such as transition metals be well below 10^{10} atoms/cm^2. Detection of this extremely low level of impurity is beyond the capability of standard RBS, and is only approached with difficulty by state-of-the-art Total Reflection X-ray Florescence (TXRF) equipment. A new IBA technique is under development which meets this requirement with a simple modification of the basic RBS approach.[14,15]

The technique, called Heavy Ion Backscattering Spectrometry (HIBS), takes advantage of the Z and energy dependence of the scattering cross-section. Note that in eq. 3 the scattering (and hence the yield) are proportional to Z^2 of the analyzing beam and inversely proportional to E^2: by using a heavier, lower energy beam, the cross-sections for heavy impurities on a surface can be increased dramatically. Changing from 2 MeV He^+ to 400 keV C^+ increases their yield by more than 200X. Unfortunately, the yield from the substrate also increases and the resultant high count rate overwhelms any trace element signal with pileup. Improvements can be made with cooled detectors and pileup rejection circuitry[16], but a simpler, more effective method is to place a thin carbon or plastic foil between the sample and the detector.[14,15] Its thickness is chosen such that particles scattered from the substrate are ranged out in the foil, while particles scattered from impurities heavier than the substrate (which have higher energy) pass through and are detected. Using this approach we have demonstrated sensitivities of $\sim 5 \times 10^{10}$ Fe/cm^2 and $\sim 10^9$ Au/cm^2 on Si. Future development of this technique should further improve these values.

An example of HIBS used in a study of the effects of metal contamination on Si microelectronics processing is shown in Fig. 5. Spectra obtained from both a very clean, epitaxially deposited Si surface and a deliberately contaminated Si surface are shown. A 300 keV C^+ beam was used, with a solid angle of 0.1 sr for the detector. The exponential background at low energy is due to system noise and to some particles backscattered from the

Si substrate which are making it through the foil in front of the detector. The contamination procedure was intended to deposit low amounts of Cu and Fe, whose measured amount is consistent with TXRF measurements of the same wafer and whose signal is seen at the edge of the background in the spectrum of Fig. 5. The peak at higher energy corresponds to 2 x 10^{11} atoms/cm^2 of an additional, unknown contaminant with mass ~140 amu, which was not detectable by TXRF. Further details of the contamination experiments and a comparison of the results to other trace element analyses is found elsewhere in these proceedings.[17]

In the mode just described, with a ranging foil in front of the detector, the detection sensitivity of HIBS for heavy impurities is as high as any other technique, but the depth and mass resolution are poor ($\Delta M \sim 10$ amu), due to straggling in the foil (that is, energy spreading of backscattered particles as they pass through the foil). Although the HIBS spectra contain depth information, just as in standard RBS, the poor resolution combined with shallow depth of analysis would be unsuitable for most applications. An alternative approach to using low energy, heavy ion beams for analysis has been explored by Mendenhall and Weller.[18-20] They have used a time-of-flight detector, without a ranging foil, to achieve much better mass and depth resolution using beams such as Li^+ in the 100-500 keV range. Although their sensitivity to trace amounts of impurities is not as good, they have demonstrated depth resolution of 2-3 nm with their technique, which they call Medium Energy Backscattering Spectrometry.

Resonant Nuclear Reaction Analysis

Nuclear Reaction Analysis, in which the probing ion beam causes a nuclear reaction with the target atom of interest, rather than scattering, has a number of possible configurations. Most are used for determining the total amount of a particular light element with relatively high sensitivity, but without the capability of extracting a depth profile. However, Resonant Nuclear Reaction Analysis (RNRA) does provide a depth profiling capability by scanning the energy of an analysis beam through a sharp resonant reaction, varying in turn the depth at which the resonance occurs. Detection of the total amount of the reaction product then corresponds to the concentration versus depth, with the depth scale provided by the usual energy loss calculations for the probe beam.

Perhaps the best example of RNRA is the use of the 6.4 MeV $^1H(^{15}N, \alpha\gamma)^{12}C$ reaction to profile hydrogen.[21] The resonance is very narrow (fwhm = 1.8 keV), and produces characteristic gamma-rays with 4.43 MeV energy. To measure a hydrogen profile, the target is bombarded with a ^{15}N beam at 6.4 MeV and above, and the gamma-rays are counted as a function of incident energy with a gamma-ray detector such as a BGO scintillator. An example of such an analysis is shown in Fig. 6,[22,23] where the hydrogen at the interface of a

deposited Au layer on Si has been profiled. This powerful analysis tool is one of the very few ways that hydrogen can be profiled in solids with high sensitivity. The main drawback to the technique is that off-resonance yield or yield from additional resonances at lower energies can interfere with the analysis.

Elastic Recoil Detection Spectrometry

A final area of IBA that has opened up new possibilities for application is ERD, which is most useful for analyzing target elements from Z=1 to 9.[24-27] A schematic of ERD is shown as an inset in Fig.7: the analysis beam for ERD is heavier than the element to be profiled and is brought into the sample at a low angle. Collisions with light elements in the target result in forward recoils of the target atoms, some of which exit the sample and are detected. Thus ERD also allows for profiling of hydrogen in solids, but with generally lower sensitivity than RNRA techniques. Often in ERD a thin range foil is placed in front of the detector to filter out scattered primary beam particles. A typical ERD spectrum is shown in Fig. 7, in which a 24 MeV Si^{+5} ion beam was used to elastically recoil H, B, and N atoms from a thin film of $B_{2.5}N$ on a Si substrate. All of the scattering cross-sections for 24 MeV Si on H, B and N are Rutherford. The scattering angle was 30° and the Si beam was incident at 15° from the surface of the sample. The sample was approximately uniform in composition with a slight gradient of decreasing hydrogen and boron toward the surface. In comparison to RNRA, this example shows the ability of ERD to give H concentration profiles with a moderate depth resolution for samples with at least 0.1 atomic percent hydrogen. Note that in contrast to RBS spectra (where the energy to depth scale conversion is the same for each element from which He is scattered), the energy to depth conversion for the recoiled H and the recoiled B are drastically different. After subtracting the N contribution to the spectrum underneath the H yield, data analysis[27] gives the concentration profiles for the B and H shown in Fig. 8. Depth resolution in ERD is more strongly affected by sample roughness than in HE-BS or RNRA as indicated by the resolution of approximately 20 nm on the H profile and 30 nm on the B profile. In general, the sensitivity of ERD is approximately 0.1 atomic percent, but this can be increased by an order of magnitude with the proper geometry and beam energy to minimize background contributions.

A more recent approach to ERD involves the use of a time-of-flight detector, combined with a solid state detector positioned at the far end of the time-of-flight system.[28,29] By using both types of detectors, in a configuration such as shown in Fig. 9(a), both the mass and energy of each recoiled particle can be measured, allowing separate depth profiles to be obtained for each light element in the target. The mass resolution achievable is such that separate profiles can be obtained even for different isotopes of the same element. Figure 9(b)

shows a 3-dimensional plot of recoil yield versus particle time-of-flight and energy, obtained from boron/carbon multilayers on Si. Each band in the figure consists of counts from one particular isotope. Projection of a band onto the energy axis gives a spectrum equivalent to ordinary ERD, but without overlapping yield from other masses, and with considerably improved energy (and depth) resolution. Figure 10 shows two such projections from another set of data obtained from an $SiO_2/SiON_X$ sample, together with approximate depth scales. The sample configuration is indicated by the inset.

Summary

The examples above give some idea of the wide variety of IBA techniques available to the materials researcher. By an appropriate choice of ion beam and energy, most sample configurations can be analyzed, perhaps with tradeoffs in optimum sensitivity, depth of analysis, or depth resolution. Table 1 summarizes the techniques most useful for depth analysis. Some other IBA techniques which have not been covered here are non-resonant Nuclear Reaction Analyses (for sensitivity, rather than depth analysis), and ion channeling, which can provide crystallographic information as a function of depth.[5] Another widely used technique is Proton-Induced X-Ray Emission (PIXE), which is valuable for quantification of total composition, but with little depth information. The reviews sited here are a good starting point to learn about these other areas.[1-5]

Acknowledgements

The authors would like to thank J.C. Banks, N.D. Wing, K.G. Minor, and D.L. Buller for invaluable technical assistance. We also thank Alain Diebold of SEMATECH for his collaboration in the continuing HIBS Si contamination studies. This work was performed at Sandia National Laboratories and supported by the U.S. Department of Energy under contract #DE-AC04-76DP00789.

References

1. *Ion Beam Handbook for Materials Analysis,* edited by J.W. Mayer and E. Rimini (Academic, New York, 1977).
2. W.-K. Chu, J.W. Mayer and M.-A. Nicolet, *Backscattering Spectrometry* (Academic, New York, 1978).
3. *Ion Beams for Materials Analysis,* edited by J.R. Bird and J.S. Williams (Academic, San Diego, 1989).
4. *High Energy and Heavy Ion Beams in Materials Analysis,*edited by J.R. Tesmer, C.J. Maggiore, M. Nastasi, J.C. Barbour and J.W. Mayer (Materials Research Society, Pittsburgh, 1990).
5. L.C. Feldman, J.W. Mayer and S.T. Picraux, *Materials Analysis by Ion Channeling* (Academic, New York, 1982).
6. E. Rutherford, Phil. Mag. **21**, 669 (1911).
7. C.G. Darwin, Phil. Mag. **28**, 499 (1914).
8. L.R. Doolittle, Nucl. Instr. and Meth. **B9**, 344 (1985).
9. M.D. Strathman, p. 183 in ref. 4.
10. T. Lauritsen and F. Ajzenberg-Selove, *Nuclear Data Sheets for ^{20}Ne, Sets 5 and 6* (National Academy of Sciences, National Research Council, 1962), p. 307.
11. J.C. Barbour, B.L. Doyle and S.M. Myers, Phys. Rev. **38,** 7005 (1988).
12. J.A. Knapp, D.M. Follstaedt and B.L.Doyle, Nucl. Instr. and Meth. **B7/8**, 38 (1985).
13. J.A. Leavitt and L.C. McIntyre, Jr., Nucl. Instr. and Meth. **B56/57**, 734 (1991).
14. B.L. Doyle, J.A. Knapp and D.L. Buller, Nucl. Instr. and Meth. **B42**, 295 (1989).
15. J.A. Knapp and B.L. Doyle, Nucl. Instr. and Meth. **B45**, 143 (1990).
16. R.R. Hart, H.L. Dunlap, A.J. Mohr and O.J. Marsh, Thin Solid Films **19**, 137 (1973).
17. A.C. Diebold, P. Maillot, M. Gordon, J. Baylis, J. Chacon, R. Witowski, H. Arlinghaus, J.A. Knapp, and B.L. Doyle, these proceedings.
18. M.H. Mendenhall and R.A. Weller, Nucl. Instr. and Meth. **B40/41**, 1239 (1989).
19. M.H. Mendenhall and R.A. Weller, Nucl. Instr. and Meth. **B47**, 193 (1990).
20. M.H. Mendenhall and R.A. Weller, Nucl. Instr. and Meth. **B59/60**, 120 (1991).
21. W.A. Lanford, H.P. Trautvetter, J. Ziegler and J. Keller, Appl. Phys. Lett. **28**, 566 (1976).
22. K.M. Horn, W.A. Lanford, K. Rodbell and P. Ficalora, Nucl. Instr. and Meth. **B26**, 559 (1987).
23. K.M. Horn and W.A. Lanford, Nucl. Instr. and Meth. **B34**, 1 (1988).
24. J. L'Ecuyer, C. Brassard, C. Cardinal and B. Terrault, Nucl. Instr. and Meth. **149**, 271 (1978).

25. J.P. Thomas, M. Fallavier, D. Ramdane, N. Chevarier and A. Chevarier, Nucl. Instr. and Meth. **218**, 125 (1983).
26. B.L. Doyle and P.S. Peercy, Appl. Phys. Lett. **34**, 811 (1979).
27. B. L. Doyle and D. K. Brice, Nucl. Instr. and Meth. **B35**, 301 (1988).
28. H.J. Whitlow, p. 73 in ref. 4.
29. J.P. Thomas, M. Fallavier and A. Ziani, Nucl. Instr. and Meth. **B15**, 443 (1986).

Table 1. IBA techniques useful for depth profiling. In the examples, the species in bold are the beam and the detected product. The HIBS row includes both high sensitivity and high resolution configurations (see text).

technique	example	beam energy (MeV)	detectable Z	depth resolution (Å)	analysis depth (μm)
RBS	$\alpha + {}^{197}Au \rightarrow \alpha + {}^{197}Au$	1-3	5-94	25-500	0.1-50
HE-BS	$\alpha + {}^{12}C \rightarrow \alpha + {}^{12}C$	3-15	1-94	200-500	3
HIBS	${}^{12}C + {}^{197}Au \rightarrow {}^{12}C + {}^{197}Au$	0.1-0.5	20-94	20 or 1000	0.5
RNRA	${}^{15}N + p \rightarrow {}^{12}C^* + \alpha$ ${}^{12}C^* \rightarrow {}^{12}C + \gamma$	0.9-15	1, odd A	10-200	1-3
ERD	${}^{28}Si + p \rightarrow p + {}^{28}Si$	2-30	1-9	50-800	0.5
TOF-ERD	${}^{197}Au + {}^{16}O \rightarrow {}^{197}Au + {}^{16}O$	2-50	1-28	15-50	0.02

Figure Captions

Fig. 1. Schematic of the basic RBS configuration.

Fig. 2. Cross-section as a function of energy for ^{4}He incident on ^{16}O.

Fig. 3. A 8.7 MeV α HE-BS spectrum from a 1.7 μm thick $EuBa_2Cu_3O_{6.9}$ film shows the enhanced yield of O, which is 22x Rutherford.[11]

Fig. 4. High-energy backscattering spectrum from Ti and C implanted Fe.[12] The C yield is 50x Rutherford. The depth scales indicated for each mass, in nm, assume the volume density of pure Fe.

Fig. 5. Plot of HIBS spectra from a clean Si surface and a Si surface deliberately contaminated by resist-dosing technique.[17]

Fig. 6. RNRA measurement of hydrogen at the interface between Si and a deposited Au layer, using the 6.4 MeV $^{1}H(^{15}N, \alpha\gamma)^{12}C$ reaction.[22]

Fig. 7. ERD spectrum obtained with a 24 MeV Si beam from a $B_{2.5}N$ layer on Si. The different widths in the spectrum for the H and B signals is due to the different stopping powers for the two recoiling species.

Fig. 8. Depth profiles for H and B extracted from the data of Fig.7. Note the different vertical scales for the two elements.

Fig. 9. (a) Schematic of a TOF-ERD experiment. (b) Yield vs. energy and time of flight for particles recoiled from a BC/Si target with a 12 MeV Au beam. Each band represents yield from a single target mass, as indicated.

Fig. 10. TOF-ERD spectra projected onto the energy axis for two masses in data obtained from an $SiO_2/SiON_X$ sample. (a) Yield from ^{16}O. (b) Yield from ^{14}N.

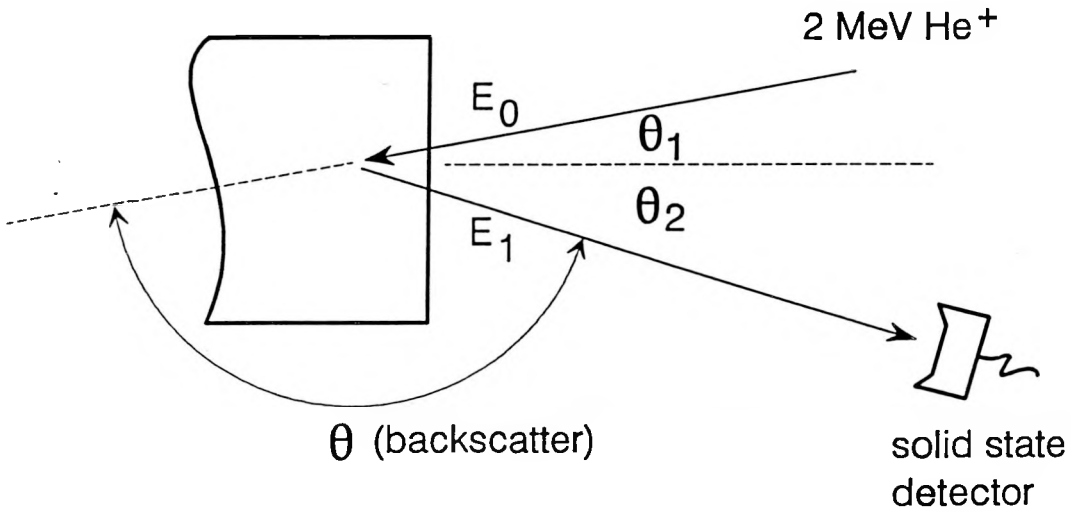

FIG. 1

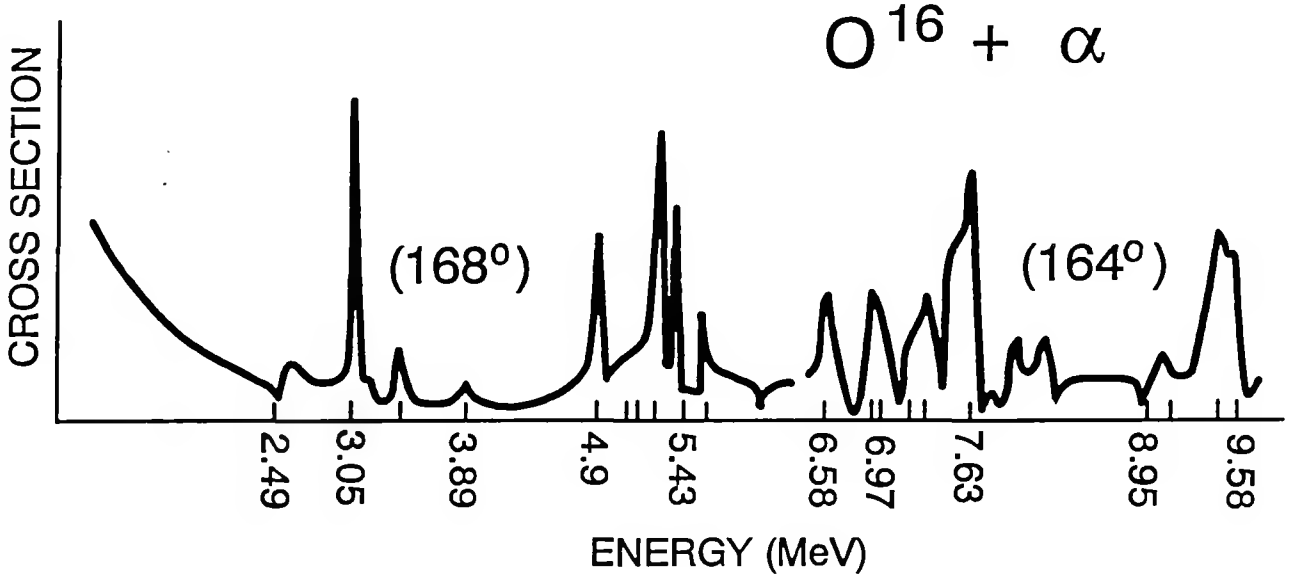
$O^{16} + \alpha$
CROSS SECTION
(168°)
(164°)
2.49
3.05
3.89
4.9
5.43
6.58
6.97
7.63
8.95
9.58
ENERGY (MeV)

FIG. 2

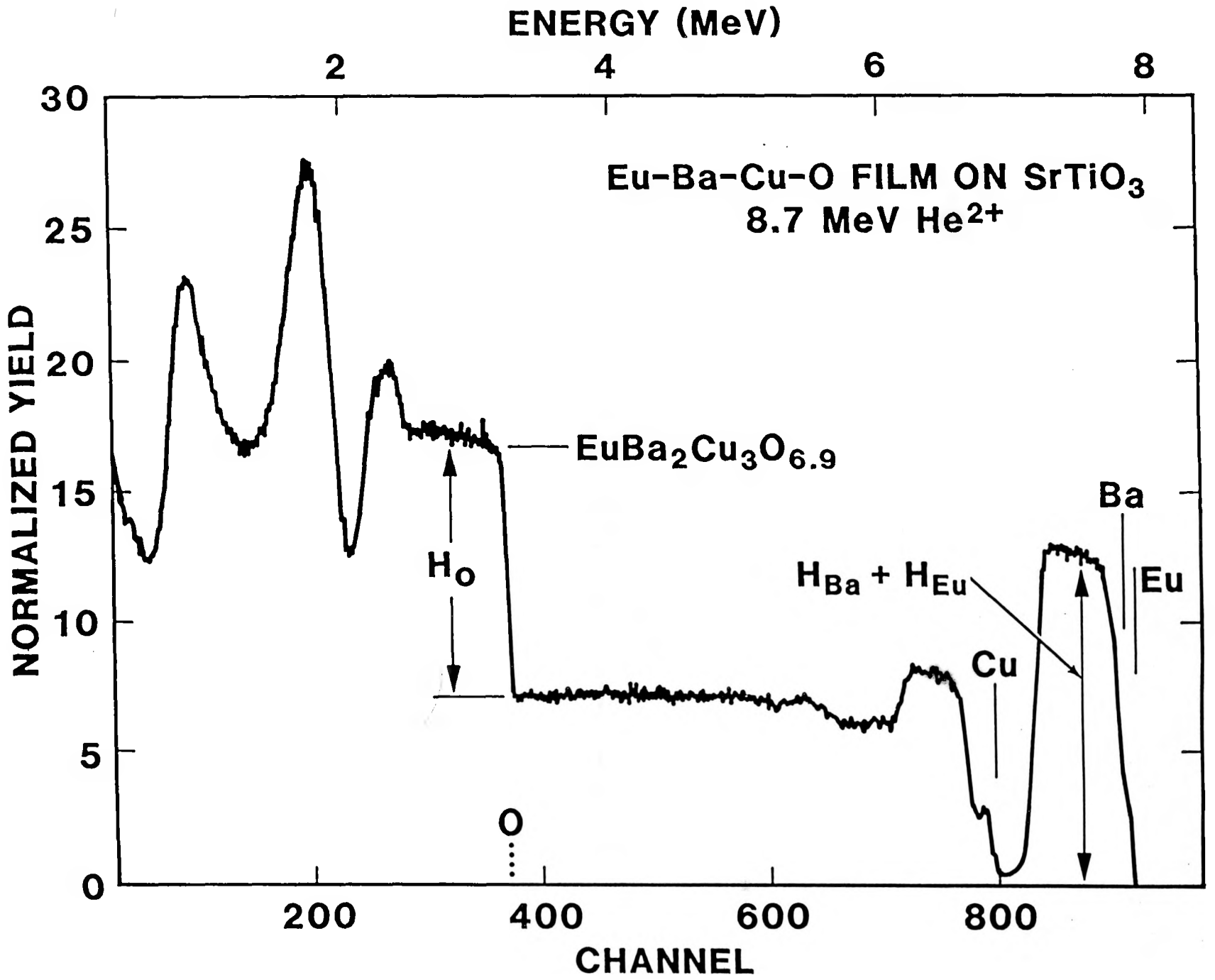
ENERGY (MeV)
2
4
6
8
30
25
20
15
10
5
0
NORMALIZED YIELD
Eu-Ba-Cu-O FILM ON SrTiO3
8.7 MeV He2+
EuBa2Cu3O6.9
Ho
HBa + HEu
Ba
Eu
Cu
O
200
400
600
800
CHANNEL

FIG. 3

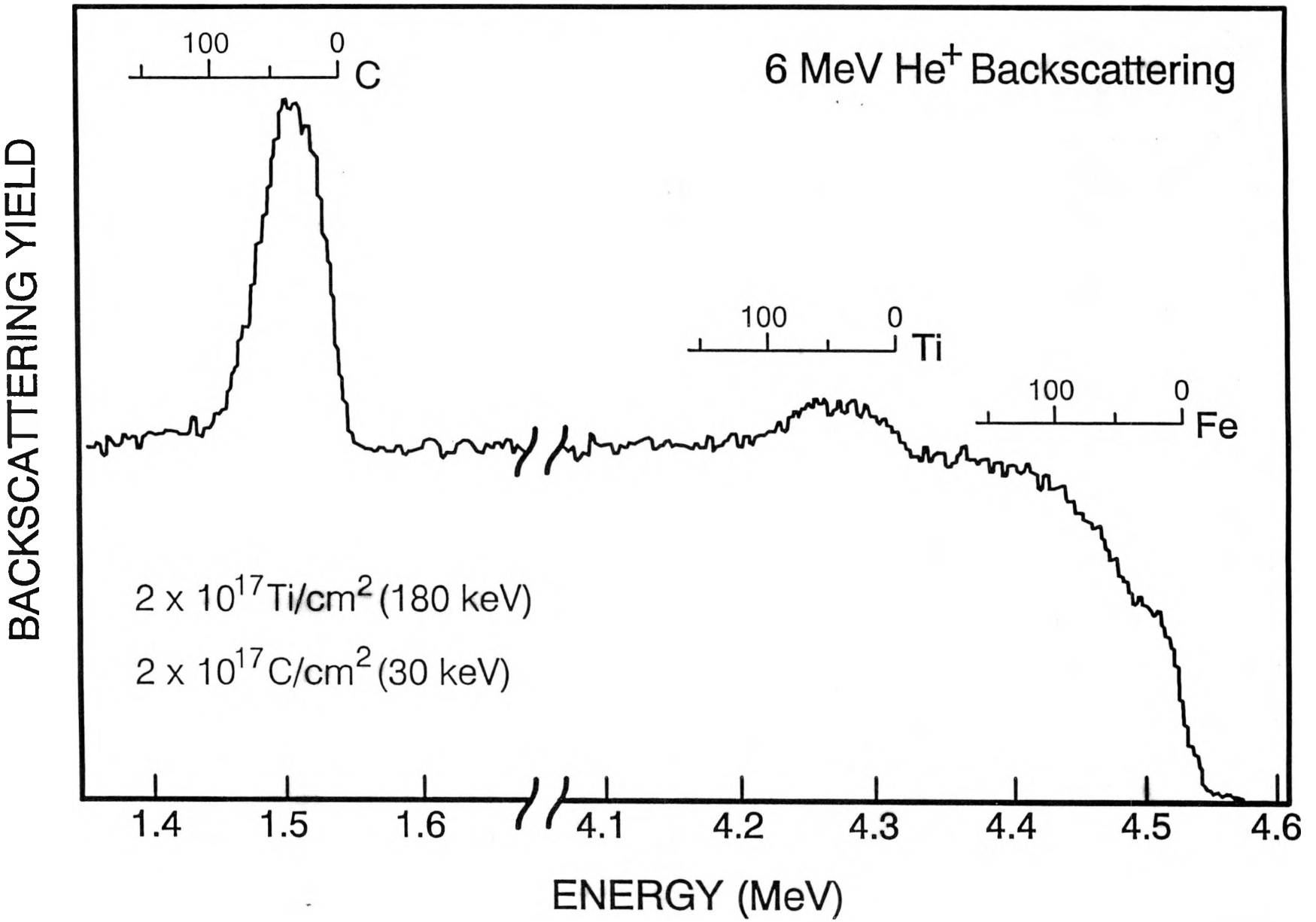
6 MeV He+ Backscattering
100
0
C
100
0
Ti
100
0
Fe
2 x 10^17 Ti/cm^2 (180 keV)
2 x 10^17 C/cm^2 (30 keV)
BACKSCATTERING YIELD
1.4
1.5
1.6
4.1
4.2
4.3
4.4
4.5
4.6
ENERGY (MeV)

Fig. 4

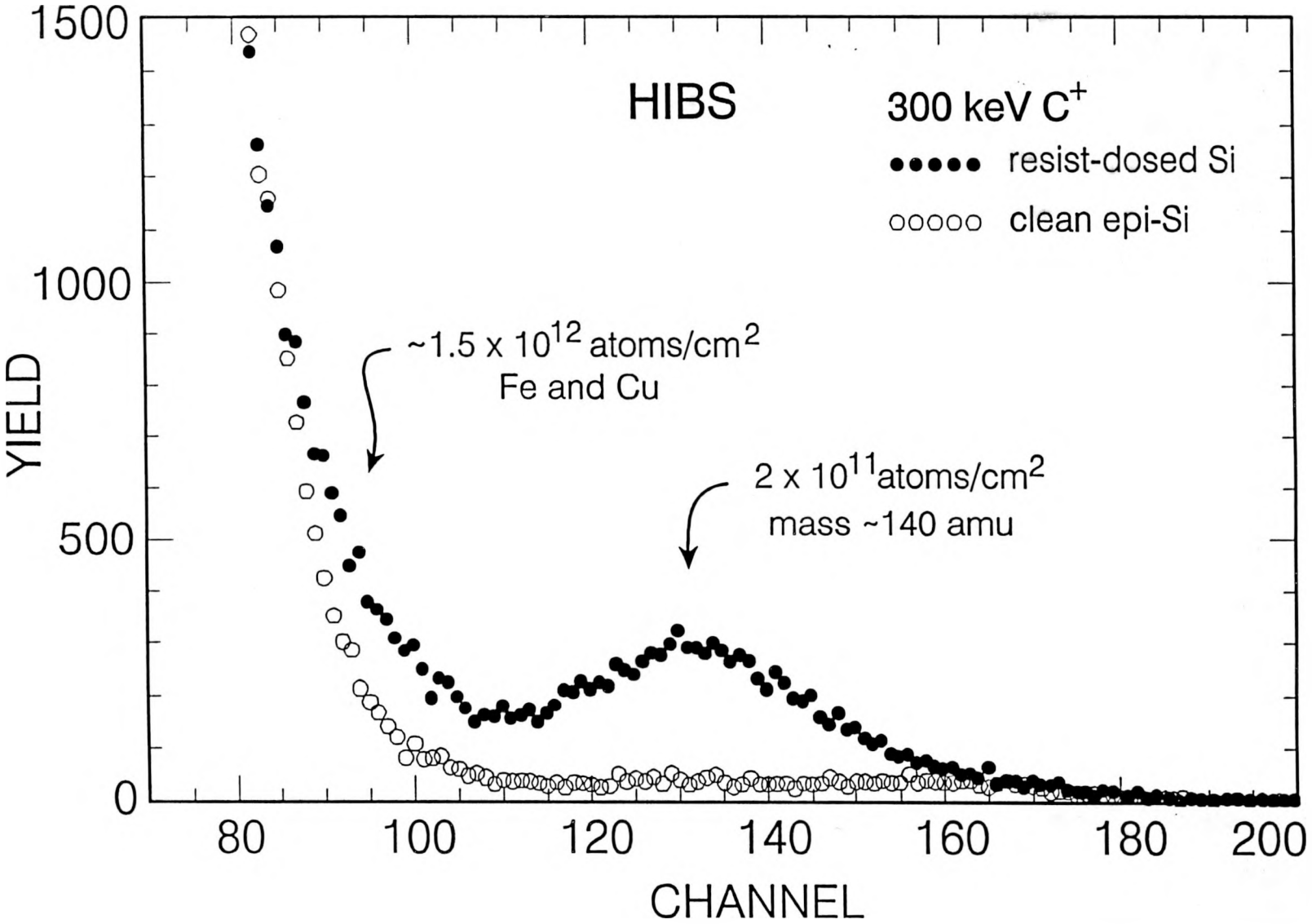
HIBS
300 keV C+
resist-dosed Si
clean epi-Si
~1.5 x 10^12 atoms/cm^2
Fe and Cu
2 x 10^11 atoms/cm^2
mass ~140 amu
YIELD
CHANNEL
1500
1000
500
0
80
100
120
140
160
180
200

Fig. 5

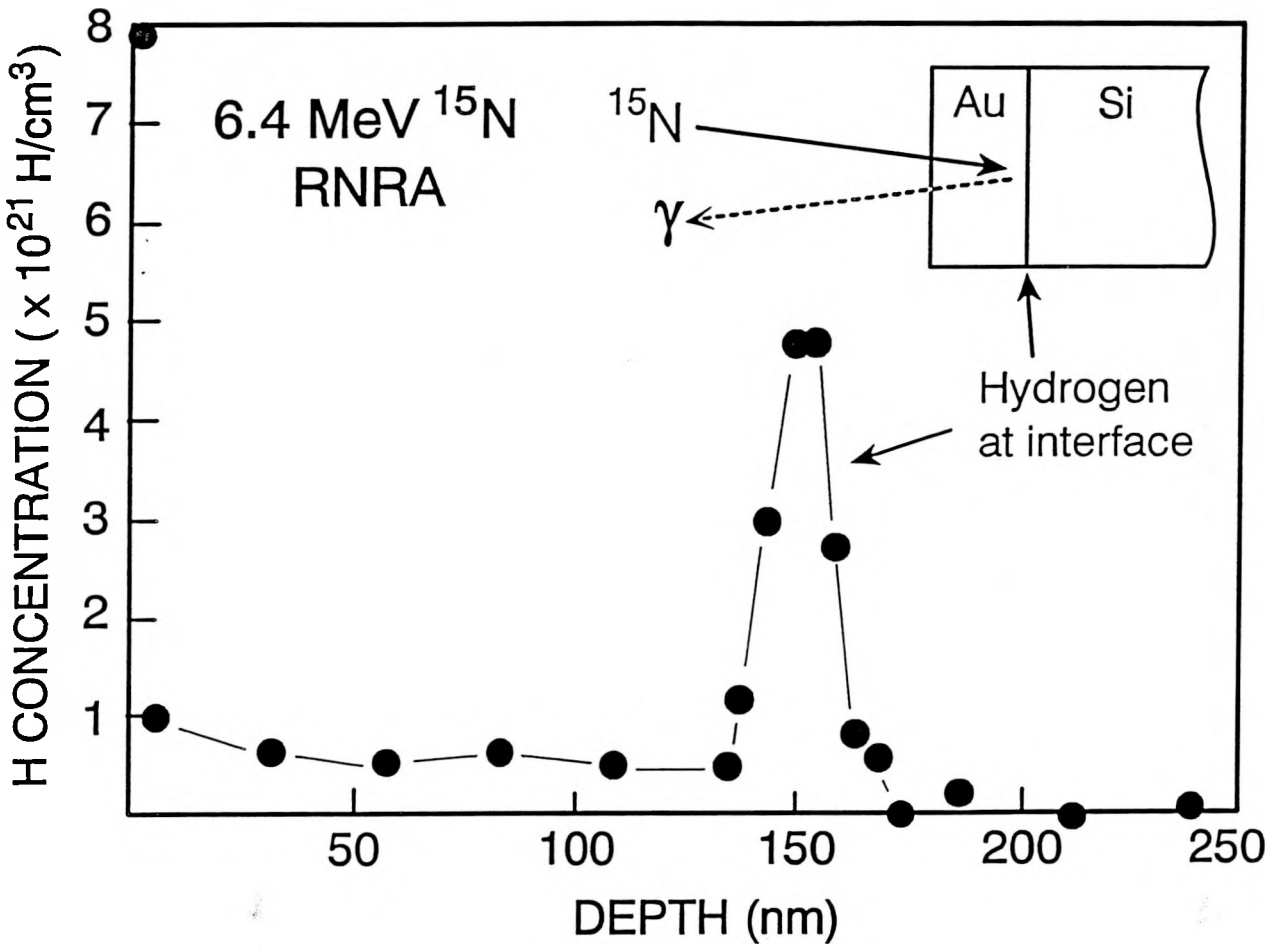
6.4 MeV ^{15}N
RNRA
^{15}N
γ
Au
Si
Hydrogen
at interface
H CONCENTRATION (x 10^{21} H/cm^3)
DEPTH (nm)
1
2
3
4
5
6
7
8
50
100
150
200
250

FIG. 6

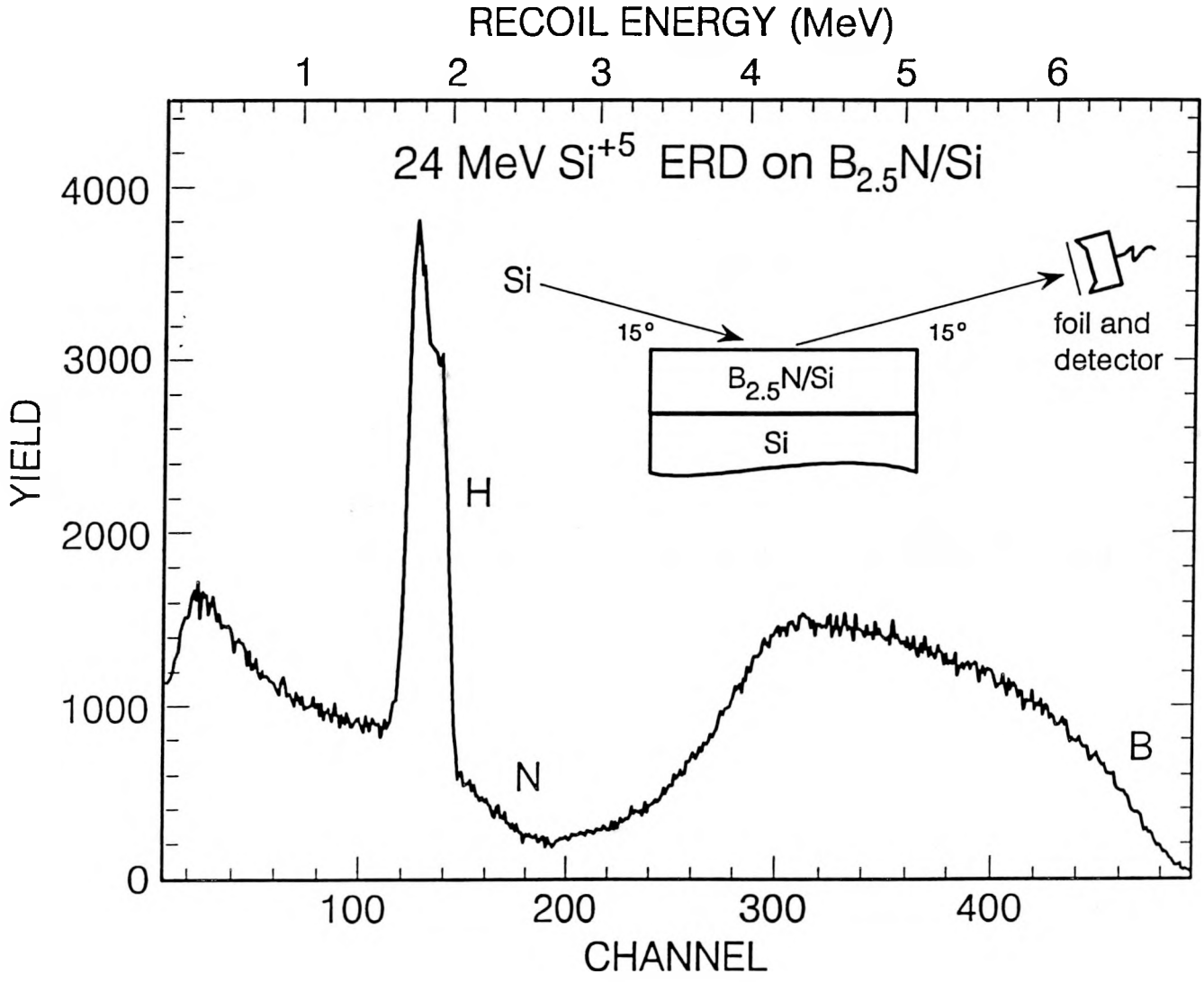
RECOIL ENERGY (MeV)
1
2
3
4
5
6
24 MeV Si+5 ERD on B2.5N/Si
Si
15°
15°
foil and
detector
B2.5N/Si
Si
H
N
B
YIELD
4000
3000
2000
1000
0
100
200
300
400
CHANNEL

FIG. 7

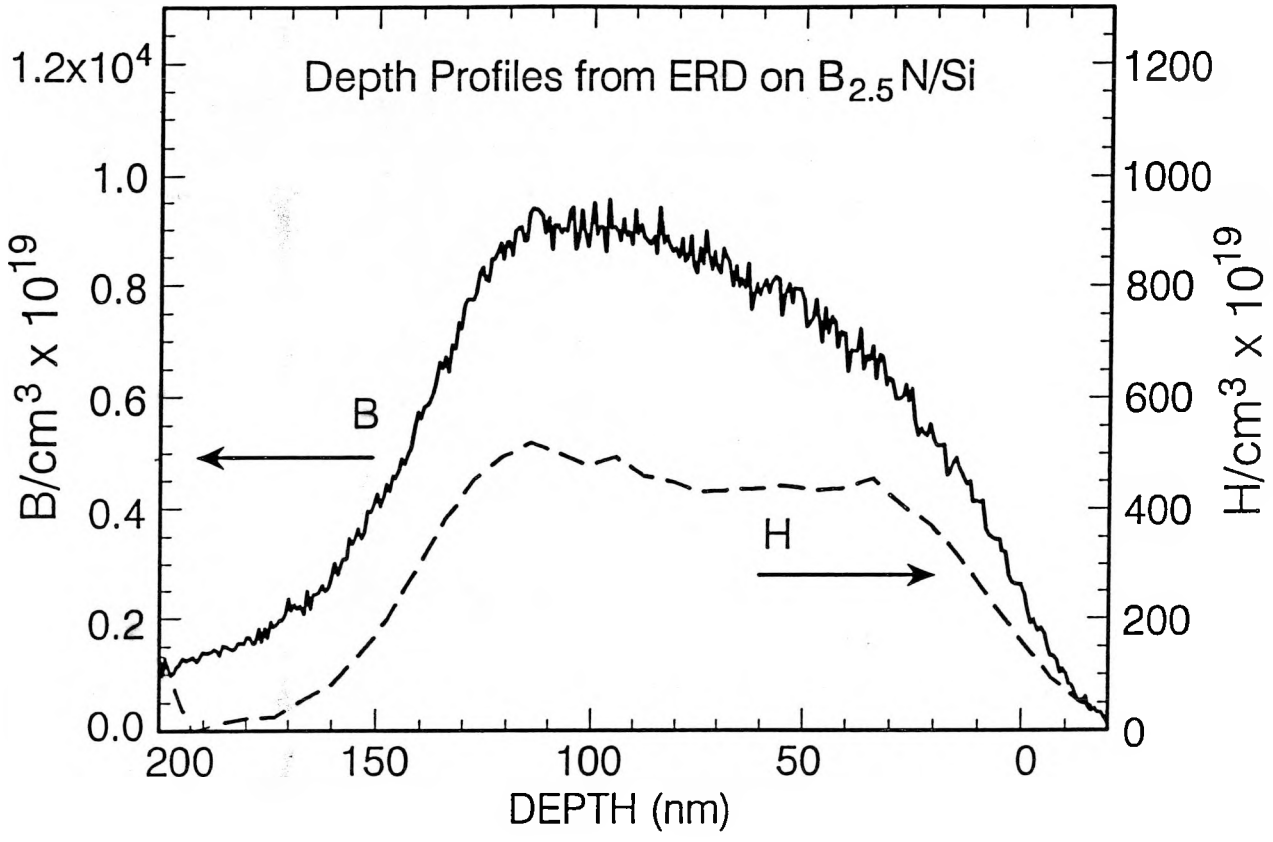
Depth Profiles from ERD on $B_{2.5}N/Si$
1.2x10^4
1.0
0.8
0.6
0.4
0.2
0.0
B/cm^3 x 10^19
1200
1000
800
600
400
200
0
H/cm^3 x 10^19
B
H
200
150
100
50
0
DEPTH (nm)

FIG. 8

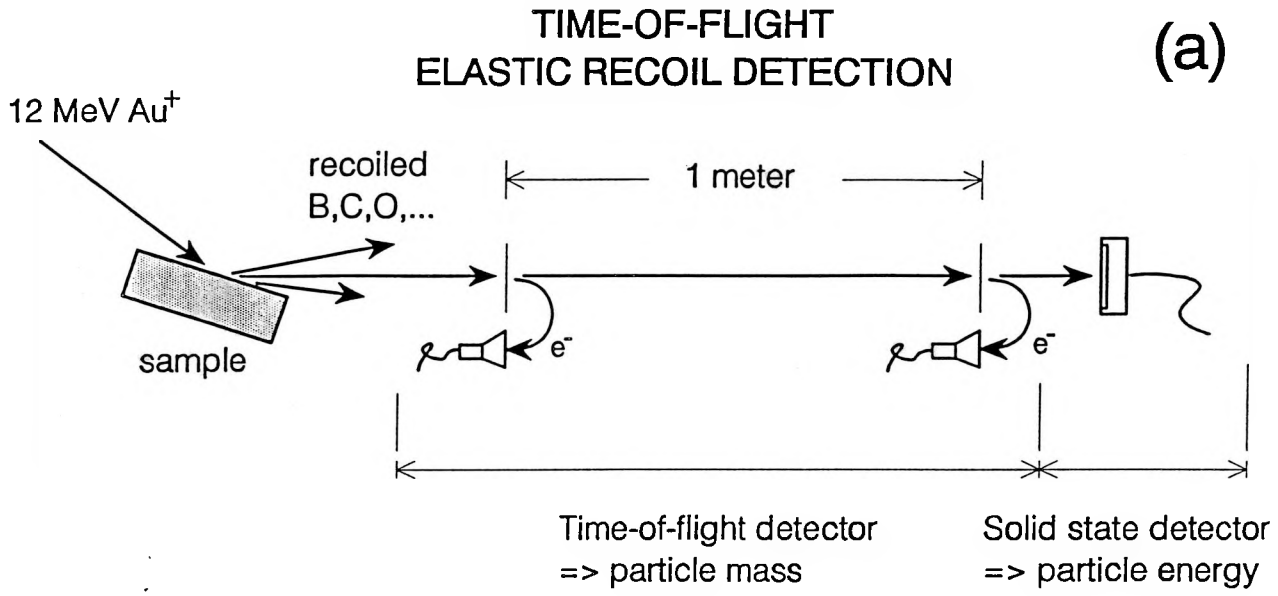
TIME-OF-FLIGHT
ELASTIC RECOIL DETECTION
(a)
12 MeV Au+
recoiled
B,C,O,...
1 meter
sample
e-
e-
Time-of-flight detector
=> particle mass
Solid state detector
=> particle energy

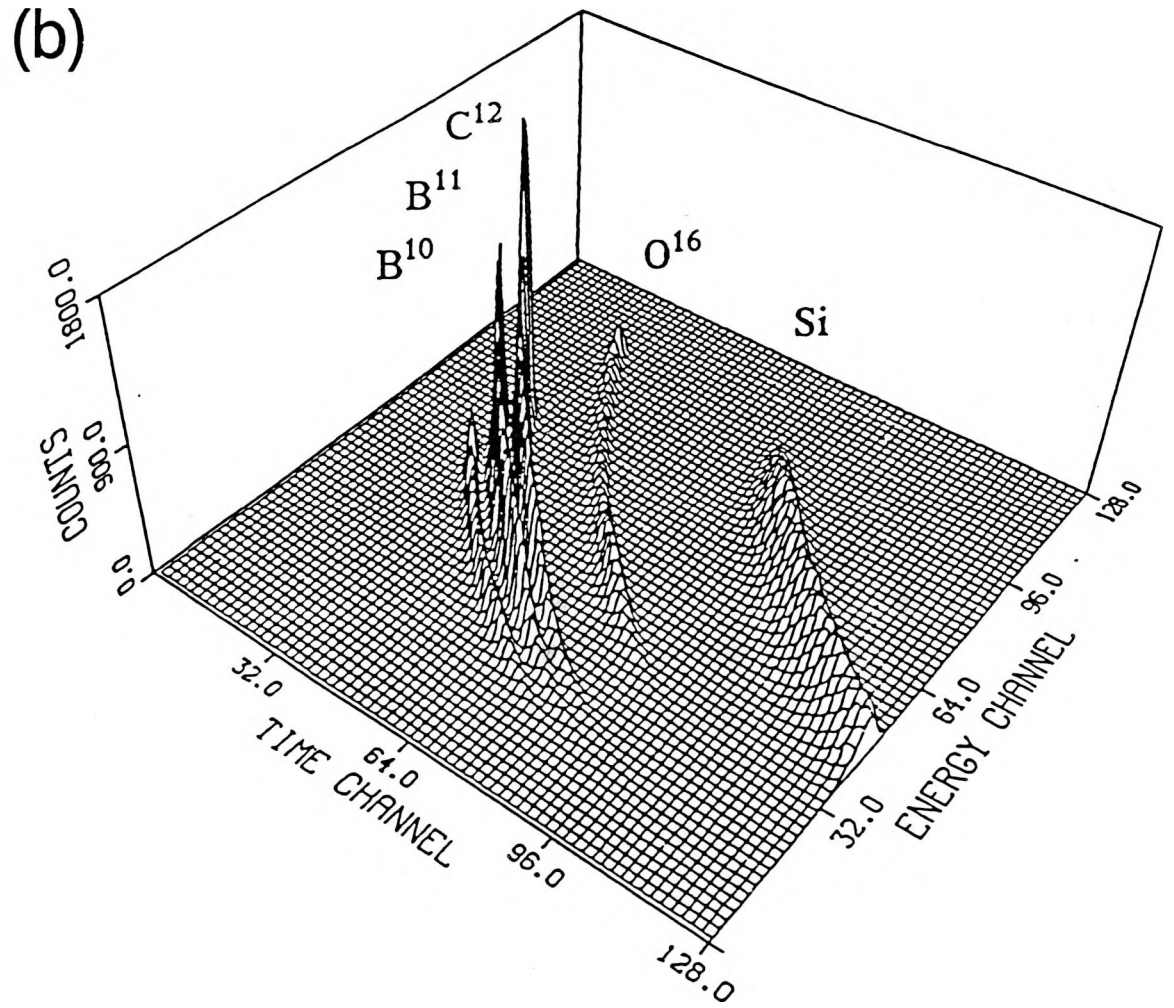
(b)
C12
B11
B10
O16
Si
COUNTS
0.0
900.0
1800.0
TIME CHANNEL
32.0
64.0
96.0
128.0
ENERGY CHANNEL
32.0
64.0
96.0
128.0

FIG. 9

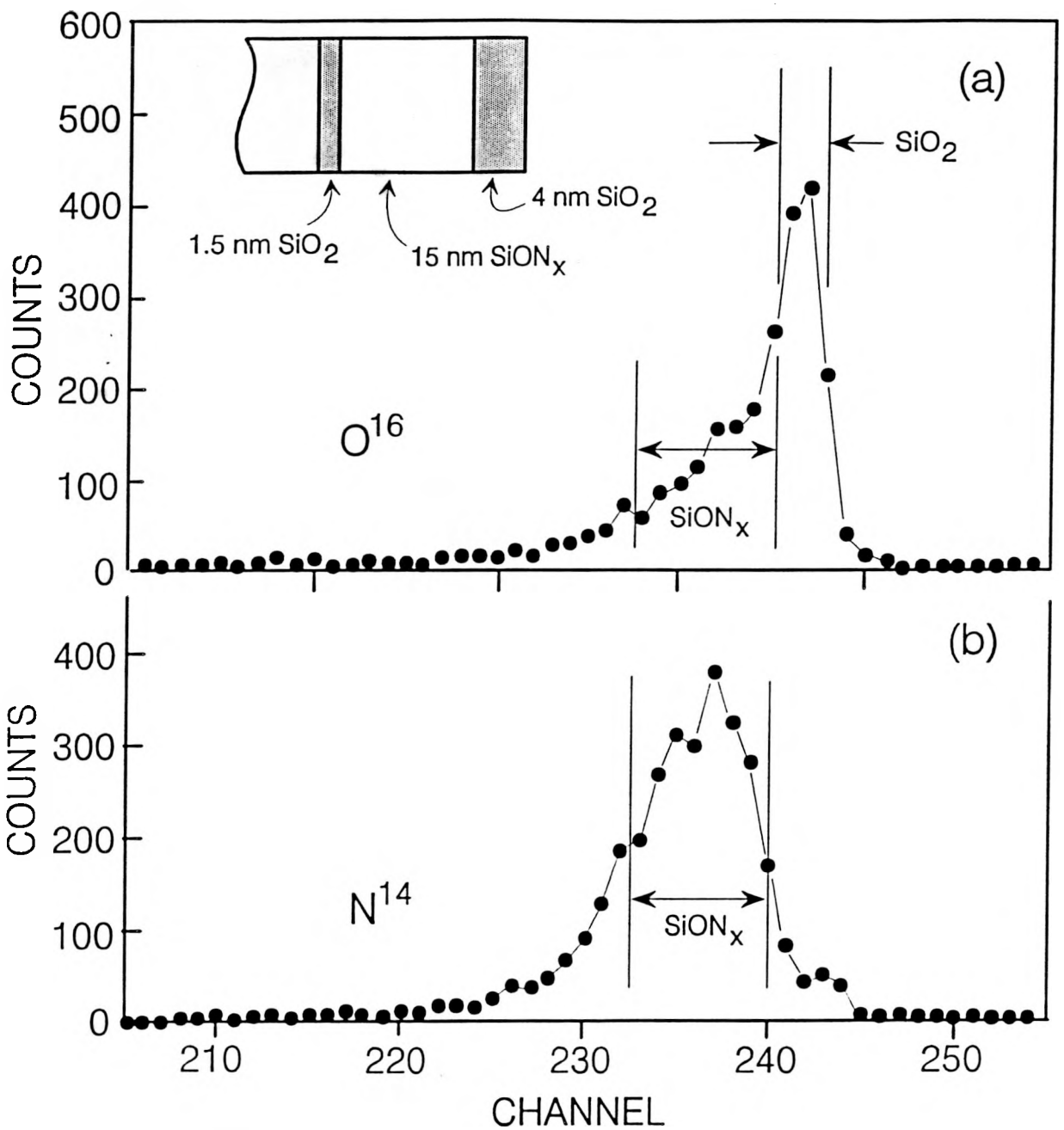
600
500
400
300
200
100
0
COUNTS
(a)
1.5 nm SiO_2
15 nm $SiON_x$
4 nm SiO_2
SiO_2
O^{16}
$SiON_x$
400
300
200
100
0
COUNTS
(b)
N^{14}
$SiON_x$
210
220
230
240
250
CHANNEL

FIG. 10